Constructing the Universe with Clusters of Galaxies, IAP 2000 meeting, Paris (France) July 2000
Florence Durret & Daniel Gerbal eds.

CLUSTER FORMATION REDSHIFTS AND THE MASS-TEMPERATURE RELATION

BENJAMIN F. MATHIESEN
Department of Physics, Stanford University, Stanford, CA 94305-4060 USA

I employ an ensemble of hydrodynamical simulations and the XSPEC MEKAL emission model to reproduce observable spectral and flux-weighted temperatures for 24 clusters. Each cluster is imaged at 16 points in its history, which allows the investigation of evolutionary effects on the mass-temperature relation. In the redshfit zero scaling relations, I find no evidence for a correlation between cluster temperatures and their formation epochs out to redshifts of 0.6. This result is is true for both observable and intrinsic intracluster medium temperatures, and implies that standard Press-Schechter theory is sufficient to describe the properties of the local X–ray temperature function.

1 Introduction

Galaxy clusters are the youngest and largest organized structures known to exist, and as such can shed light on many cosmological problems. They arise from significantly overdense regions on cosmological scales, which are exponentially rare events in a Gaussian random initial perturbation spectrum. The shape and normalization of the cluster mass function are therefore extremely sensitive to the statistical properties of the primordial density field. The evolution of cluster number densities is also tightly coupled to cosmic expansion during the epoch of cluster formation (and therefore Ω_m).

Much effort has been expended towards the interpretation of cluster mass functions at low and high redshifts; recent works include Eke et al.[1]; Sadat, Blanchard, & Oukbir[2]; Viana & Liddle[3]; Borgani et al.[4]; Reichart et al.[5]; and Henry[6]. A number of observational programs are also underway to assemble large-scale surveys of the cluster population at high redshifts (Thompson, Willick, & Mathiesen, this conference; Romer et al.[7], Holden et al.[8], Gladders & Yee[9]). The goal of placing precise constraints on Ω_m by measuring the evolution of the cluster mass function is common to all these programs, but much remains to be understood about the clusters themselves before we can be confident of results arising from this method.

The properties of the local mass function can be constrained by using either standard Press-Schecter[10] (also Bond et al.[11], Lacey & Cole[12]) theory, a more sophisticated analytical model of the cosmic mass function (e.g. Sheth, Mo, & Tormen[13]), or fitting formula based on large-scale structure simulations (Jenkins et al.[14]). Such models predict the number density of dark matter haloes as a function of mass and redshift. Some relationship between model variables (i.e., the total mass within some density threshold) and a more easily observed quantity (e.g. X–ray temperature, X–ray luminosity, or weak lensing mass) must therefore be assumed to match cosmological predictions to the results of cluster surveys. Intracluster medium (ICM) X–ray temperatures show particular promise in this regard, since they demonstrate a tight ($\lesssim$ 20%) correlation with cluster mass components in both simulations (Mathiesen & Evrard[15], total virial masses) and observations (Mohr, Mathiesen, & Evrard[16], ICM virial masses), and the cluster X–ray temperature function (XTF) currently provides the tightest constraints on the cluster mass function. ICM temperatures are also relatively easy to measure, and the next generation of mass function contraints are likely to come from medium-redshift ($0.4 < z < 0.6$) *Chandra* or *XMM* observations. It is therefore essential to make sure that our interpretation of the local cluster temperature function is correct.

A modified form of the mass function based on the difference between a cluster's formation redshift and observed redshift was first proposed by Kitayama & Suto[17], and has begun to be commonly implemented in deriving constraints on the power spectrum normalization σ_8 at low redshfits (Kitayama & Suto[18], Kay & Bower[19], Viana & Liddle[3]). This extension to the theory produces little change in the shape of the predicted mass function, but can have an appreciable effect on the predicted temperature function if one assumes that clusters evolve along a mass-temperature scaling relation appropriate to their formation redshift. It is therefore assumed that cluster histories contain a objectively identifiable formation event, during which the majority of the observed cluster mass coalesced for the first time and the intracluster medium virialized at a temperature appropriate to the halo mass and formation epoch. These assumptions are reasonable in the framework of standard Press-Schechter theory, but perhaps pay too little heed to the more complicated, hydrodynamical evolution of the ICM. They are also testable using two-fluid simulations of cluster formation.

The goal of this paper is to investigate the evolution of intrinsic and observable cluster temperatures using an ensemble of 24 hydrodynamic cluster simulations, and test the appropriateness of this extension to the interpretation of cluster temperature functions. In the following section I describe the ensemble of simulated clusters and our model for the ICM X–ray emission. In section 3, I look for evidence of temperature evolution of our ensemble. Section 4 sums up and discusses the results. The Hubble constant is parameterized as $H_0 = 100h^{-1}$ km s^{-1} Mpc^{-1}.

2 SPH Simulations and Observable Temperatures

We use an ensemble of 24 hydrodynamical cluster simulations, divided evenly between two reasonable cold dark matter (CDM) cosmological models. These models are (i) OCDM ($\Omega_0 = 0.3$, $\sigma_8 = 1.0$, $h = 0.8$, $\Gamma = 0.24$); and (ii) ΛCDM ($\Omega_0 = 0.3$, $\lambda_0 = 0.7$, $\sigma_8 = 1.0$, $h = 0.8$, $\Gamma = 0.24$). Here σ_8 is the linearly evolved, present day power spectrum normalization on $8h^{-1}$ Mpc scales. The initial conditions are Gaussian random fields consistent with a CDM transfer function with the specified Γ (e.g. Bond & Efstathiou[20]). The baryon density is set in each case to 20% of the total mass density ($\Omega_b = 0.2\Omega_0$). The simulation scheme is P3MSPH: the first stage is a P^{3}M (dark matter only) simulation to find cluster formation sites in a large volume, and the second stage resimulates the formation of individual clusters with higher resolution. Smoothed particle hydrodynamics (SPH) is included in the individual cluster simulations to resolve the ICM structure in detail. The baryonic component is modeled with 32^3 particles, providing a typical mass resolution of 0.01% within the virial radius. The resulting cluster sample covers a little more than a decade in total mass, ranging from about 10^{14} to $3 \times 10^{15} M_\odot$. These simulations were first presented a paper describing the cluster size-temperature relation (Mohr & Evrard[21]).

The simulations model the dynamical and thermodynamical effects of gravitation, shock heating and adiabatic work on the ICM. Several potentially important pieces of physics are neglected. Radiative cooling is perhaps the most significant; our clusters cannot produce cooling flows in their cores. Cooling flows have the potential to greatly influence measurements of the ICM core luminosity and temperature, but the energy loss due to radiation is small compared to that released in the process of gravitational collapse. We therefore expect that the results of these simulations are comparable to observational results which attempt to account for the presence of cooling flows, either through excision or explicit modeling of excess core emission. Other neglected processes include galaxy feedback (Metzler & Evrard[22]) which can create abundance gradients and shallower gas profiles; preheating of the ICM (Cavaliere, Menci, & Tozzi[23]; Lloyd-Davies, Ponman, & Cannon[24]), which can raise the ICM entropy and limit the density of baryonic cores; and electron temperature lag, which slightly cools X–ray spectra in rich clusters (Chièze, Alimi & Teyssier[25]; Takizawa[26]) relative to the ion temperature. Further discussion of these issues in terms of their relevance to cluster simulations can be found in Mathiesen & Evrard[15] (hereafter ME01).

In ME01 we introduced an ensemble of spectrally and spatially resolved X–ray surface brightness images derived from these simulations. We used the MEKAL (Mewe, Lemen, & van den Oord[27]) emission model from the XSPEC utility, since this is the one most commonly used by to interpret observed ICM spectra. Each SPH particle was assigned a 0.3 solar metallicity spectrum scaled to its density and thermodynamic temperature, binned in 50 eV intervals over the [0.1,20] keV bandpass. The clusters were then "observed" by collecting photons in a circular window centered on the minimum potential of the cluster, and a combined spectrum was produced which incorporates emission from gas at a wide variety of densities and temperatures. We produced *Chandra*-like combined spectra and spectral images by adopting 150 eV bins, a 0.5-9.5 keV bandpass, and finally convolving the photon distribution with *Chandra's* effective area function and a moderate (3.4×10^{20} cm^{-2}) absorbing column density. The physical scale of the observation windows used in this paper varies from cluster to cluster, but usually corresponds to a fixed mean interior overdensity of 500 times the critical density appropriate to the redshift and cosmological model. This radius is labeled r_{500}, and is a fixed fraction of the virial radius in any cosmology. The radius r_{200} is also used in this work, but corresponds less closely to observable regions of the ICM.

The resulting spectra are surprisingly similar in character to isothermal spectra with a temperature typically 10-20% lower than the mass-weighted, thermodynamic temperature of the cluster. A semantic separation of the two concepts appears to be necessary, so hereafter we refer to the *Chandra*-like temperature just described as a *spectral* temperature, T_s. The mass-weighted, thermodynamic temperature of the ICM in these simulations will be referred to as the *virial* temperature T_v, because this measure is found to follow the virial relation $M_{\rm tot} \propto T^{1.5}$ quite precisely in the simulations. T_v is identical to the mass-weighted temperature T_m described in ME01. When spectral fitting is limited to the 2.0-9.5 keV band (a bandpass similar to most published temperature determinations) the deviation between spectral temperature and virial temperature follows the relation

$$\delta T_s \equiv \frac{T_v - T_s}{T_s} = (0.19 \pm 0.06) \log_{10} T_s[\mathrm{keV}] - (0.02 \pm 0.04). \tag{1}$$

The scale-dependence of δT_s steepens the observed mass-temperature relation to $M_{\rm tot} \propto T_s^{1.62}$, and implies that rich clusters are probably more massive than their spectral temperatures would lead us to believe. The difference between spectral and virial temperatures arises partly from the presence of multiple phases in any given gas column, and partly from intrinsic ICM temperature profiles. Both of these effects contribute cool gas to the observation window and an overabundance of soft line-emission photons to the spectrum. I refer the reader to ME01 for further details on this work; the exact mass–temperature relations derived from these simulations are listed there, and will be repeated here when they are used.

The temperature bias described in Equation 1 has a potentially important effect on any interpretation of the cluster temperature function and its evolution. As has already been stated, these simulations do not include radiative cooling and are therefore directly comparable only to X–ray data which has accounted for the presence of cooling flows through excision or explicit modeling of the excess emission. Since it has not been possible until very recently to measure the spatial extent of cooling flows in high-redshift clusters, most studies of cluster evolution have evaluated the temperature and luminosity functions at low redshifts without attempting such corrections. In such works, the additional scatter introduced into cluster scaling relations by cooling flows has been accepted as a source of uncertainty in the cosmological constraints.

With the advent of *Chandra* and *XMM*, however, we can do better. Markevitch[28] has shown that by excising the central $50h^{-1}$ Mpc of nearby clusters and including a cooling flow component in the core spectrum, the scatter in the luminosity-temperature relation can be reduced by a factor of two. This allows for a more robust calculation of the maximum observable volume for each cluster, as well as providing a cleaner estimate of the ICM temperature in cooling flow clusters. Spatially resolved spectroscopy should allow similar corrections to be made in high-redshift clusters. In order to acheive precise cosmological constraints from a measurement of evolution in the cluster temperature function, it is therefore desirable to model such cooling flow-corrected temperatures.

Temperatures derived from high-quality *ASCA* data (Markevtich et al.[29]) are commonly used in constructing the local XTF or measuring the slope of cluster scaling relations. These are flux-weighted mean spectral temperatures, which in principle should be biased towards regions of dense and/or cool gas (at fixed density, a 1 keV gas parcel will emit more photons than a 10 keV gas parcel). This measure was found by Markevitch to produce a significant shift in cooling flow cluster temperatures relative to a simpler, isothermal fit to the combined spectrum. Non-cooling flow cluster temperatures, on the other hand, were more or less unchanged.

Such temperatures are difficult to reproduce precisely in the simulations, mainly because the spatial extent and pixelization of *ASCA* images is different for each cluster in the sample.[29] The large scale of *ASCA* spectral regions implies that the temperatures in each pixel are similar in character to the spectral temperatures described earlier, but with more weight given to the luminous core than the outer regions. I simulate these temperatures by dividing our observation windows into nine sectors with a morphology typical for *ASCA* clusters: a core region with radius $r_{500}/4$; an inner annulus surrounding this region with outer radius $5r_{500}/8$, and an outer annulus surrounding this region with outer radius r_{500}. The two annuli are each divided into 4 quadrants. The spectral temperature T_s in each sector is weighted by it's total energy flux. This temperature will be referred to as a *flux-weighted* temperature for the remainder of this paper, and given the label T_f. This definition of the temperature should not be confused with the emission-weighted temperature T_e described in ME01, which is the density-weighted average thermodynamic temperature calculated over a spherical volume. T_f is, however, closely comparable to the emission-weighted temperatures described in Markevitch's analysis of *ASCA* clusters.

The deviation between the observable flux-weighted temperature T_f and the virial temperature T_v has a slope similar to that reported in Equation 1, but a different normalization:

$$\delta T_f \equiv \frac{T_v - T_f}{T_f} = (0.22 \pm 0.05) \log_{10} T_f[\mathrm{keV}] - (0.11 \pm 0.03). \tag{2}$$

The slope of the flux-weighted temperature bias is similar to that of the spectral temperature bias, and leads to an observable mass-temperature relation having a slope of 1.66. This is significantly steeper than the virial relation, and is consistent with the spectral temperature relation reported in ME01. T_f is higher than T_s because of the extra weight given to the core. The deviation δT_f ranges from about -10% to +10% for clusters with virial temperatures ranging from 1 to 10 keV. Calculating the flux-weighted mean temperature over a coarse grid does not

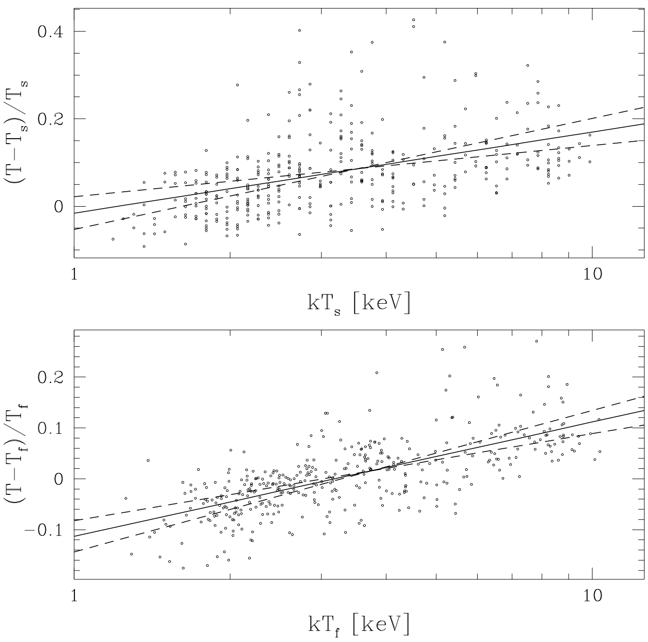

Figure 1: The upper panel displays the deviation δT_s between virial temperature and spectral temperature as a function of the spectral temperature. 384 points are displayed, corresponding to 16 evolutionary epochs of 24 independent cluster simulations. The best-fit correlation between δT_s and T_s is independent of redshift. The lower panel displays the same relationship, but using the flux-weighted temperature T_f rather than the spectral temperature. The dashed lines in each panel display one-sigma variations on the best-fit correlation.

free temperature measurements of a spectral bias due to the presence of multiple densities and temperatures in a gas column, but it does provide a more accurate estimate of the virial temperature for all but the smallest clusters.

The deviations between virial temperature and observable spectral temperatures described in Equations 1 and 2 do not vary with cosmological model or evolutionary epoch, nor do they vary significantly when the radius of the observed region is increased to enclose an mean overdensity of 200 times the critical density. The deviations δT_s and δT_f are displayed in Figure 1. These are robust measures of an observational bias arising from the multiple densities and temperatures present in a typical ICM gas column. SPH simulations have been shown to accurately reproduce the large-scale morphology of real clusters (Mohr, Evrard, Fabricant, & Geller[30]), and a similar analysis of this particular ensemble displayed an even closer structural correspondence (Mohr & Evrard, private communication). N-body simulations of dark matter evolution have likewise been shown to produce merger histories which are in good agreement with Press-Schechter theory (Lacey & Cole[31]), so it is likely that these variations are similar in magnitude to those in real clusters. Analysis of Eulerian simulations reveals a similar level of clumping in the ICM (Bryan & Norman, private communication).

3 The Evidence for Temperature Evolution

A standard assumption in converting a cluster mass function $n(M,z)$ to an observable XTF $n(T,z)$ is that the redshift of the clusters is equivalent to their formation epoch. Kitayama & Suto[17] were the first to present an extension to the theory which accounted for this discrepancy, applying the techniques of Lacey & Cole[12] to the problem of calculating a realistic distribution of formation epochs to the objects at a given redshift. Their underlying assumption was that clusters which virialized significantly earlier than their observation epoch would be hotter than clusters of a similar mass which collapsed more recently. Cosmological scaling of the background mean density and temperature predicts a normalization evolution in the mass-temperature relation proportional to $h(z)/h_0 = \sqrt{\Omega_{\rm m}(1+z)^3 + \Omega_\Lambda}$ for a flat universe (e.g. Bryan & Norman[32]). The possibility of additional evolution in cluster temperatures due to unknown ICM physics also exists. Other groups have recently begun to take up this standard in modeling the temperature function and its evolution (Viana & Liddle[3], Kay & Bower[19]).

Making this correction implies an additional assumption, however: that the X–ray luminous regions of clusters are approximately relaxed. Merger events have the potential to significantly alter a cluster's temperature when they occur, and they need not be very large to do so (Cavaliere, Menci, & Tozzi[33], ME01). For a cluster which formed at high redshift to maintain a temperature appropriate for that epoch, it should have already accumulated most of its observed mass. The rate of mergers observed in simulations makes this scenario seem unlikely, although Kitayama and Suto cite results from Eulerian simulations (Bryan & Norman[32]) indicating that a cluster's temperature doesn't change much after its formation. We note that the temperature which they refer to is a simulation's luminosity-weighted temperature (similar to the T_e used in ME01), which is very similar to the core temperature of the gas. Observational measures of the temperature such as T_s and T_f are more heavily influenced by cool gas in the outer regions of the cluster, and are therefore more susceptible to minor merger events.

These simulations can be used to test the sensitivity of observable and virial temperatures to ongoing minor mergers. The mass of our clusters as a function of flux-weighted temperature is plotted in Figure 2, and presents a tight correlation with only 18% scatter around the best-fit relation,

$$\log_{10}(M_{\rm tot} h(z)) = (1.66 \pm 0.04) \log_{10} T_f + (13.59 \pm 0.02). \tag{3}$$

This plot combines cluster outputs at redshifts $z = 1.0$, 0.5, and 0. The small degree of scatter in this plot strongly implies that there is no significant contamination of the temperature ensemble by clusters which virialized early; when scaled to a similar epoch the three scaling relations $M(T_f)$ are identical. We can, however, probe this issue more deeply.

We define a cluster's formation epoch z_f as the redshift at which it has acquired $75\% \pm 7.5\%$ of its final mass, following the convention used by Viana & Liddle[3] in their most recent paper constraining cosmological parameters. If the extension of Kitayama and Suto is relevant to our interpretation of the local XTF, then we should see a correlation between cluster temperature and z_f; the clusters with a high formation redshift should on average have temperatures higher than the mean mass-temperature relation. Figure 3 plots this difference for the virial, spectral, and flux-weighted temperatures within observation windows of radius r_{500} and r_{200}. Error bars along the z_f axis are given to objects which passed through the mass threshold with a significant component of continuous accretion, so that the cluster had between 67.5% and 82.5% of its final mass in more than one output frame. The uncertainties which are implied by these error bars are not used in statistical analysis of these data. The best-fit lines to the four data sets are all consistent with zero, although it is also fair to say that there is evidence for a slight positive correlation indicating that clusters which formed earlier do have somewhat higher temperatures. On the other hand, this correlation is largely driven by the rare clusters which formed at very high redshifts; most of these objects formed at $z_f < 0.6$ and are evenly distributed about the mean mass-temperature relationship. While we don't have enough clusters in the ensemble to place a limit on the level of contamination, these data certainly seem consistent with no correction.

Correlation coefficients and best-fit line parameters for each of these data sets are summarized in Table 1. The correlations within r_{200} are significantly influenced by a cluster with a formation redshift of 0.8 and very large error bars on that value. This cluster acquired most of its mass very early in the simulation and grew through gradual accretion thereafter, so the reshift range during which it had a mass of $75\% \pm 7.5\%$ its final mass is very long. It's tem-

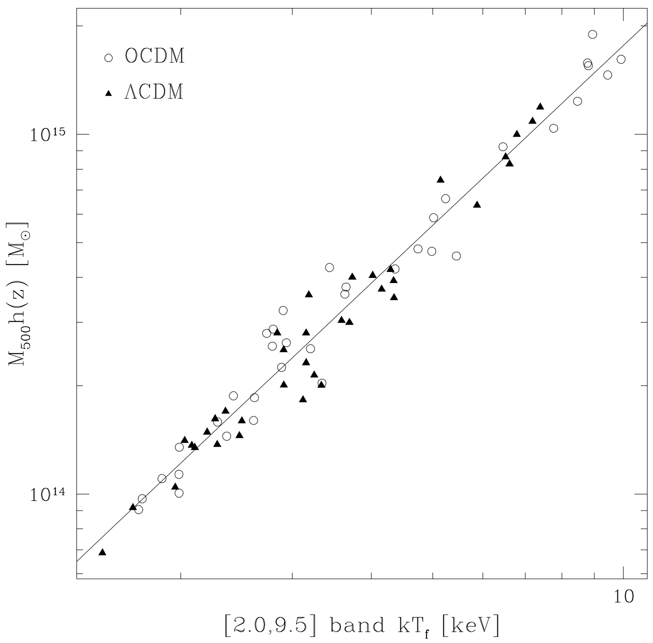

Figure 2: The relationship between flux-weighted temperature T_f and total mass measured within r_{500}. Clusters at redshifts 0.0, 0.5 and 1.0 are included in the plot, with masses scaled by the cosmological evolution factor h(z). The best-fit relation is drawn, and its parameters are reported in Equation 3.

Window	Temperature	R	slope	intercept
r_{200}	T	0.31(15%)	0.060 ± 0.044	-0.018 ± 0.017
	T_s	0.28(20%)	0.080 ± 0.066	-0.024 ± 0.025
	T_f	0.12(58%)	0.030 ± 0.060	-0.009 ± 0.022
r_{500}	T	0.21(33%)	0.041 ± 0.051	-0.014 ± 0.020
	T_s	0.28(20%)	0.078 ± 0.086	-0.026 ± 0.034
	T_f	0.11(68%)	0.024 ± 0.057	-0.008 ± 0.022

Table 1: A correlation analysis of the data presented in Figure 3. R is the correlation coefficient of the data, and is also translated into the probability that an uncorrelated set of 24 random points would produce a correlation coefficient at least that large. The slope and intercept of the best-fit lines plotting in Figure 3 are also given.

perature, while higher than the ensemble average, is well within the variations seen for more recently formed clusters. If this point is left out the analysis, then all the best-fit slopes become consistent with zero in their one-sigma uncertainty range, and the correlation coefficients of the r_{200} data drop to 0.24 (T_v), 0.19 (T_s), and 0.005 (T_f). These coefficients correspond respectively to 32%, 39%, and 100% probabilities of uncorrelated data.

The discrepancy between our intuition (clusters which first virialized at an early epoch should be hotter) and these simulations can be resolved by acknowledging the essentially dynamic nature of clusters in a low-density universe. Multiple lines of observational evidence point to an $\Omega_m \sim 0.3$ cosmology in which clusters are still forming at the present day, and the theoretical construct of a relaxed, virialized cluster seems to have few counterparts in the observable population. Rather than treating clusters as static fossils of the primordial density field, we should attempt to model them explicitly as evolving entities. One example of such a model has been presented by Cavaliere, Menci, & Tozzi[33], who analyze ICM structure in terms of "punctuated equilibrium", a sequence of merger shocks followed by partial relaxation of the ICM to the shock boundary conditions. Their model agrees with these simulations in showing that minor merger events

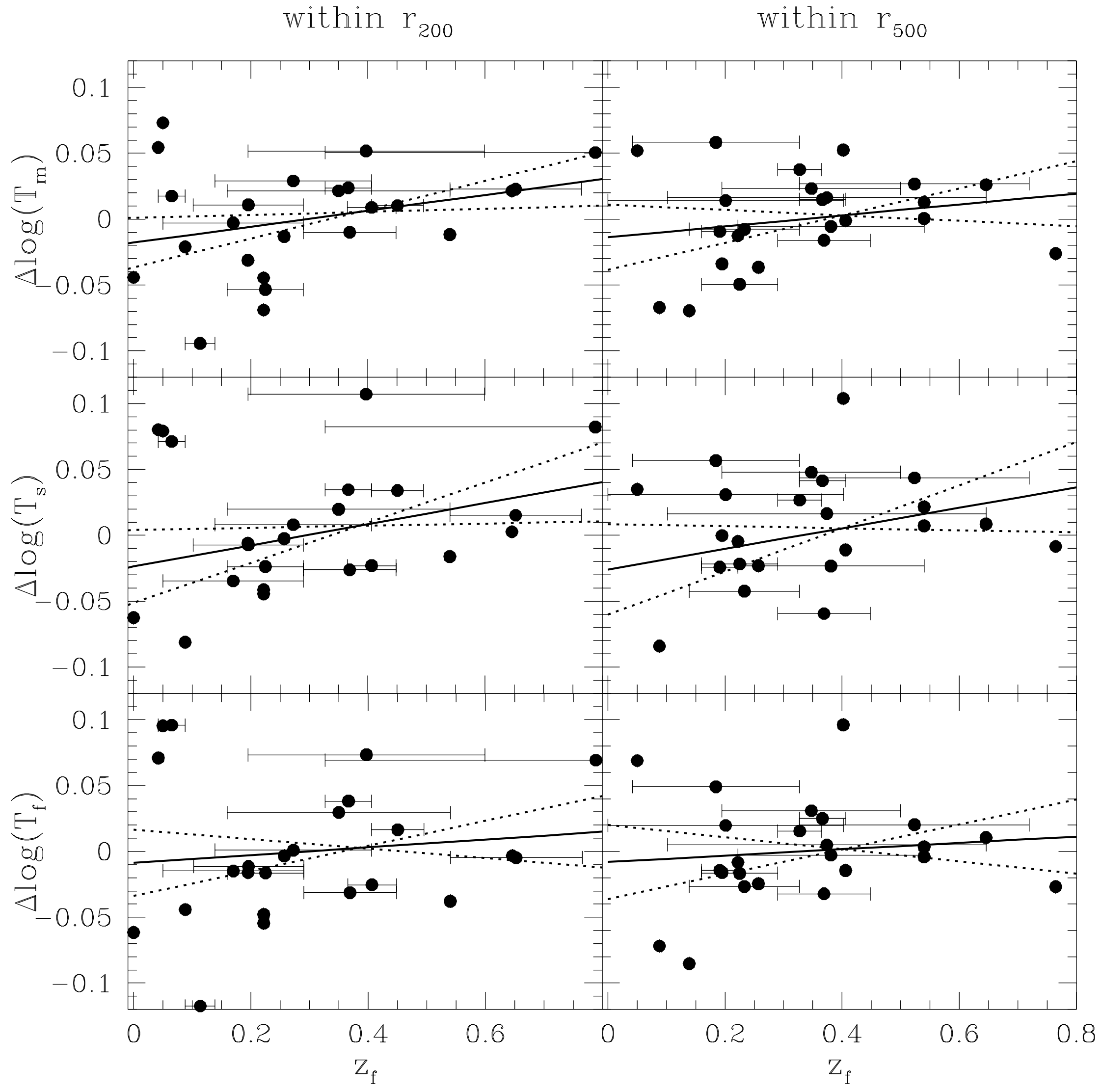

Figure 3: The best-fit mass-temperature relationship $\bar{T}(M)$ is calculated for the 24 clusters in the ensemble at a redshift of zero, and the deviation of individual clusters from this relation $\Delta \log T \equiv log(T/\bar{T})$ is plotted against their formation redshift z_f. Three definitions of the temperature (virial, spectral, and flux-weighted) and two observation windows are examined. If the temperature of a cluster were strongly influenced by its formation epoch, we would expect to see a correlation between $\Delta \log T$ and z_f. The evidence for correlation in this data set is marginal at best, and negligible for the flux-weighted temperatures used by Markevitch. Although these simulated clusters display cosmological evolution in the normalization of the mass-temperature relation, the mass-temperature relation at a redshift of zero does not appear to be contaminated by clusters which virialized at earlier epochs.

should have a more important influence on the evolution of ICM temperatures than major mergers. Their work also makes some important predictions about the behavior of ICM scaling relations in rich groups and poor clusters.

4 Conclusions

An analysis of the evolutionary history of simulated clusters shows only a slight dependence of cluster temperature on formation epoch out to $z_{\mathrm{f}} \sim 0.6$, although the small number of clusters in this ensemble leaves open the possibility of evolution in the temperatures of clusters which formed at higher redshifts. It is also worth reiterating that when using a flux-weighted temperature T_f, which is the definition most appropriate to analysis of the cluster temperature function, this correlation essentially vanishes. This lack of dependence on formation epoch can be traced to a high frequency of smaller ($\lesssim 25\%$) merger events carrying cool gas, which disturb the ICM and allow it to approach an equilibrium appropriate to the merger epoch. This work implies that extending Press-Schechter analysis to account for the difference between a cluster's formation time and observation time is not necessary in a dynamically young halo population.

Acknowledgments

I would like to thank Joseph J. Mohr, Keith L. Thompson, and Jeffrey A. Willick for valuable discussions which greatly aided this work. This research was supported by a Terman Fellowship and the Research Corporation.

References

1. Eke V. R., Cole S., Frenk C. S., & Henry J. P., 1998, MNRAS, 298, 1145
2. Sadat R., Blanchard A., & Oukbir J., 1998, A&A, 329, 21
3. Viana P. T. P. & Liddle A. R., 1999, MNRAS, 303, 535
4. Borgani S., Rosati P., Tozzi P., & Norman C., 1999, ApJ, 517, 40
5. Reichart D. E., Nichol R. C., Castander F. J., Burke D. J., Romer A. K., Holden B. P., Collins C. A., & Ulmer M. P., 1999, ApJ, 518, 521
6. Henry, J. P., 2000, ApJ, 534, 565
7. Romer A. K, Viana P. T. P., Liddle A. R., Mann R. G., 1999, preprint (astro-ph/9911449)
8. Holden B. P., Nichol R. C., Romer A. K., Metevier A., Postman M., Ulmer M. P., Lubin L. M., 1999, AJ, 118, 2002
9. Gladders M. D. & Yee H. K. C., preprint (astro-ph/0002340)
10. Press W. H. & Schechter P., 1974, ApJ, 187, 425
11. Bond J. R., Cole S., Efstathiou G., & Kaiser N., 1991, ApJ, 379, 440
12. Lacey C. & Cole S., 1993, MNRAS, 262, 627
13. Sheth R. K., Mo H. J., & Tormen G., 1999, preprint (astro-ph/9907024)
14. Jenkins A., Frenk C. S., White S. D. M., Colberg J. M., Cole S., Evrard A. E., & Yoshida N., 2000, preprint (astro-ph/0005260)
15. Mathiesen B. F. & Evrard A. E., 2001, ApJ, in press (astro-ph/0004309)
16. Mohr J. J., Mathiesen B. F., & Evrard A. E., 1999, ApJ, 517, 627
17. Kitayama T. & Suto Y., 1996, ApJ, 469, 480
18. Kitayama T. & Suto Y., 1997, ApJ, 490, 557
19. Kay S. T. & Bower R. G., 1999, MNRAS, 308, 664
20. Bond J. R. & Efstathiou G., 1984, ApJL, 285, L45
21. Mohr J. J. & Evrard A. E., 1997, ApJ, 491, 38
22. Metzler C. A. & Evrard A. E., 1994, ApJ, 437, 564

23. Cavaliere A., Menci N., & Tozzi P., 1998, ApJ, 501, 493
24. Lloyd-Davies E. J., Ponman T. J. & Cannon D. B., 2000, MNRAS, 315, 689
25. Chièze J.-P., Alimi J.-M. & Teyssier R., 1998, ApJ, 495, 630
26. Takizawa, M. 1999, ApJ, 520, 514
27. Mewe R., Lemen J. R., & van den Oord G. H. J., 1986, A&AS, 65, 511
28. Markevitch M., 1998, ApJ, 504, 27
29. Markevtich M., Forman W. R., Sarazin C. L., & Vikhlinin A., 1998, ApJ, 503, 77
30. Mohr J. J., Evrard A. E., Fabricant D. G., & Geller M. J., 1995, ApJ, 447, 8
31. Lacey C. & Cole S., 1994, MNRAS, 271, 676
32. Bryan G. L. & Norman M. L., 1998, ApJ, 495, 80
33. Cavaliere A., Menci N., & Tozzi P., 1999, MNRAS, 308, 599